AMERICAN SOCIETY FOR MICROBIOLOGY | mBio®

RESEARCH ARTICLE
Host-Microbe Biology

Genomic Identification of the TOR Signaling Pathway as a Target of the Plant Alkaloid Antofine in the Phytopathogen *Fusarium graminearum*

Christopher Mogg,[a] Christopher Bonner,[b] Li Wang,[b] Johann Schernthaner,[b] Myron Smith,[c] Darrell Desveaux,[d] Rajagopal Subramaniam[b]

[a]Donnelly Centre for Cellular and Biomolecular Research, University of Toronto, Toronto, Ontario, Canada
[b]Agriculture and Agri-Food Canada, Ottawa, Ontario, Canada
[c]Department of Biology, Carleton University, Ottawa, Ontario, Canada
[d]Department of Cell and Systems Biology, University of Toronto, Toronto, Ontario, Canada

ABSTRACT Antofine, a phenanthroindolizidine alkaloid, is a bioactive natural product isolated from milkweeds that exhibits numerous biological activities, including anticancer, antimicrobial, antiviral, and anti-inflammatory properties. However, the direct targets and mode of action of antofine have not been determined. In this report, we show that antofine displays antifungal properties against the phytopathogen *Fusarium graminearum*, the cause of *Fusarium* head blight disease (FHB). FHB does devastating damage to agriculture, causing billions of dollars in economic losses annually. We therefore sought to understand the mode of action of antofine in *F. graminearum* using insights from yeast chemical genomic screens. We used haploinsufficiency profiling (HIP) to identify putative targets of antofine in yeast and identified three candidate targets, two of which had homologs in *F. graminearum*. The *Fusarium* homologues of two targets, glutamate dehydrogenase (*Fg*GDH) and resistance to rapamycin deletion 2 (*Fg*RRD2), can bind antofine. Of the two genes, only the *Fgrrd2* knockout displayed a loss of virulence in wheat, indicating that RRD2 is an antivirulence target of antofine in *F. graminearum*. Mechanistically, we demonstrate that antofine disrupts the interaction between *Fg*RRD2 and *Fg*Tap42, which is part of the Tap42-phosphatase complex in the target of rapamycin (TOR) signaling pathway, a central regulator of cell growth in eukaryotes and a pathway of extensive study for controlling numerous pathologies.

IMPORTANCE *Fusarium* head blight caused by the fungal pathogen *Fusarium graminearum* is a devastating disease of cereal crops worldwide, with limited effective chemical treatments available. Here we show that the natural alkaloid compound antofine can inhibit fusarium head blight in wheat. Using yeast genomic screening, we identified the TOR pathway component RRD2 as a target of antofine that is also required for *F. graminearum* pathogenicity.

KEYWORDS *Fusarium*, drug targets, rapamycin

Antofine belongs to the phenanthroindolizidine class of alkaloids that are produced by relatives of the milkweed family (*Apocynaceae* subfamily *Asclepiadoideae*), which include *Vincetoxicum* spp., as well as members of the related genus *Tylophora* (1). These compounds have received significant attention as candidate anticancer agents, which promote apoptosis in cancer cell lines by inhibiting nuclear factor-kappa B (NF-κB) (2). Antofine has also been shown to suppress DNA and suppress cell cycle arrest as well as endosomal signaling (3, 4). More recently, the compound has been shown to inhibit angiogenesis in endothelial cells (5). Specifically, vascular endothelial growth factor (VEGF),

Citation Mogg C, Bonner C, Wang L, Schernthaner J, Smith M, Desveaux D, Subramaniam R. 2019. Genomic identification of the TOR signaling pathway as a target of the plant alkaloid antofine in the phytopathogen *Fusarium graminearum*. mBio 10:e00792-19. https://doi.org/10.1128/mBio.00792-19.

Editor James W. Kronstad, University of British Columbia

Address correspondence to Darrell Desveaux, Darrell.desveaux@utoronto.ca, or Rajagopal Subramaniam, subramaniamra@agr.gc.ca.

C.M. and C.B. contributed equally to this article.

Received 27 March 2019
Accepted 8 May 2019
Published 11 June 2019

which stimulates angiogenesis through the action of protein kinase B or AKT/mTOR signaling pathways, is inhibited by antofine via an unknown mechanism (5).

Antofine has also been shown to inhibit growth of a variety of microorganisms, including two strains of the phytopathogen *Fusarium graminearum* (6), which causes *Fusarium* head blight (FHB) disease in small-grain cereals, resulting in low-yield, low-quality, mycotoxin-contaminated grain, which poses a serious threat to food safety and the economy (7). Due to the ubiquitous global distribution of *F. graminearum*, most agronomic practices aimed at controlling FHB, including chemical control, offer only moderate control and do not eliminate the proliferation of the disease. Only a few active ingredients have been registered to suppress *F. graminearum* as a foliar or seed treatment in cereals (8). Most of these compounds belong to the triazole group of fungicides and include tebuconazole, triticonazole, difenoconazole, and ipconazole. The efficacy of these fungicides can vary between *Fusarium* species, and moreover, emergence of fungicide-resistant strains is compelling stakeholders to develop new strategies to combat FHB disease (9, 10).

Although ubiquitous in eukaryotes, only recently has the TOR signaling pathway been documented to play a role in *F. graminearum* development and pathogenesis (11). Inhibition of TOR signaling by rapamycin, which binds Fkbp12 to inhibit Tor kinase and the downstream Tap42 protein phosphatase complex, reduces both vegetative growth and conidial germination, leading to reduced pathogenicity (11). In addition, two peptidyl-proly *cis*/*trans*-isomerases, RRD1 (FGSG_09229) and RRD2 (FGSG_01092), which regulate the activity of type 2A phosphatases of the TOR pathway and confer resistance to rapamycin when mutated (12), have overlapping functions in mycotoxin production and virulence, as well as growth and reproduction (13). However, the severity of growth defects and asexual spore production are more pronounced in the *F. graminearum rrd2* (*Fgrrd2*) mutant than *Fgrrd1* (13). In addition, *Fg*RRD2, but not *Fg*RRD1, modulates sensitivity to the phenylpyrrole fungicide fludioxonil and plays a dominant role in regulation of the high-osmolarity glycerol (HOG) pathway in *F. graminearum* (13).

In this report, we use yeast haploinsufficiency profiling (HIP) to identify potential targets of antofine. We show that RRD2 is a target of antofine in *F. graminearum*. Additionally, we show that binding of antofine to RRD2 leads to the disruption of the Tap42 phosphatase complex, providing a potential mechanism for disruption of the TOR signaling pathway.

RESULTS AND DISCUSSION

We purified antofine from *Vincetoxicum* to homogeneity as previously described (see Fig. S1A in the supplemental material) (6). After establishing a standard growth curve based on spore concentrations (Fig. S1B) and a linear relationship between mycelial growth and weight (Fig. S1C), we showed that antofine suppressed *F. graminearum* germination and growth in a dose-dependent manner with a 50% inhibitory concentration (IC_{50}) of ~100 μg/ml (see Fig. S2A in the supplemental material). Tylophorine is structurally related to antofine, and both compounds display similar activities, including growth inhibition of many cancer cell lines by blocking S-phase transition and arresting HepG2, HONE-1, and NUCG-3 carcinoma cells at the G_1 phase (14). However, the suppression of *F. graminearum* germination and growth (as well as yeast growth [Fig. 1B]) was specific to antofine, and we therefore used tylophorine as a biologically inactive negative control (Fig. 1A) (15). In addition to suppressing *in vitro* growth, antofine decreased FHB symptoms on wheat heads when coinoculated with *F. graminearum* spores (Fig. S2B). It should be noted that at the antofine concentrations tested, antofine alone did not produce any observable deleterious effects such as kernel weight (data not shown).

In order to identify potential targets of antofine, we used haploinsufficiency profiling (HIP) in yeast (16). HIP exploits drug-induced haploinsufficiency, as measured by growth defects resulting from deletion of one copy of a drug target gene, and has been used to identify the targets of small molecules, including fungicides (16). After establishing

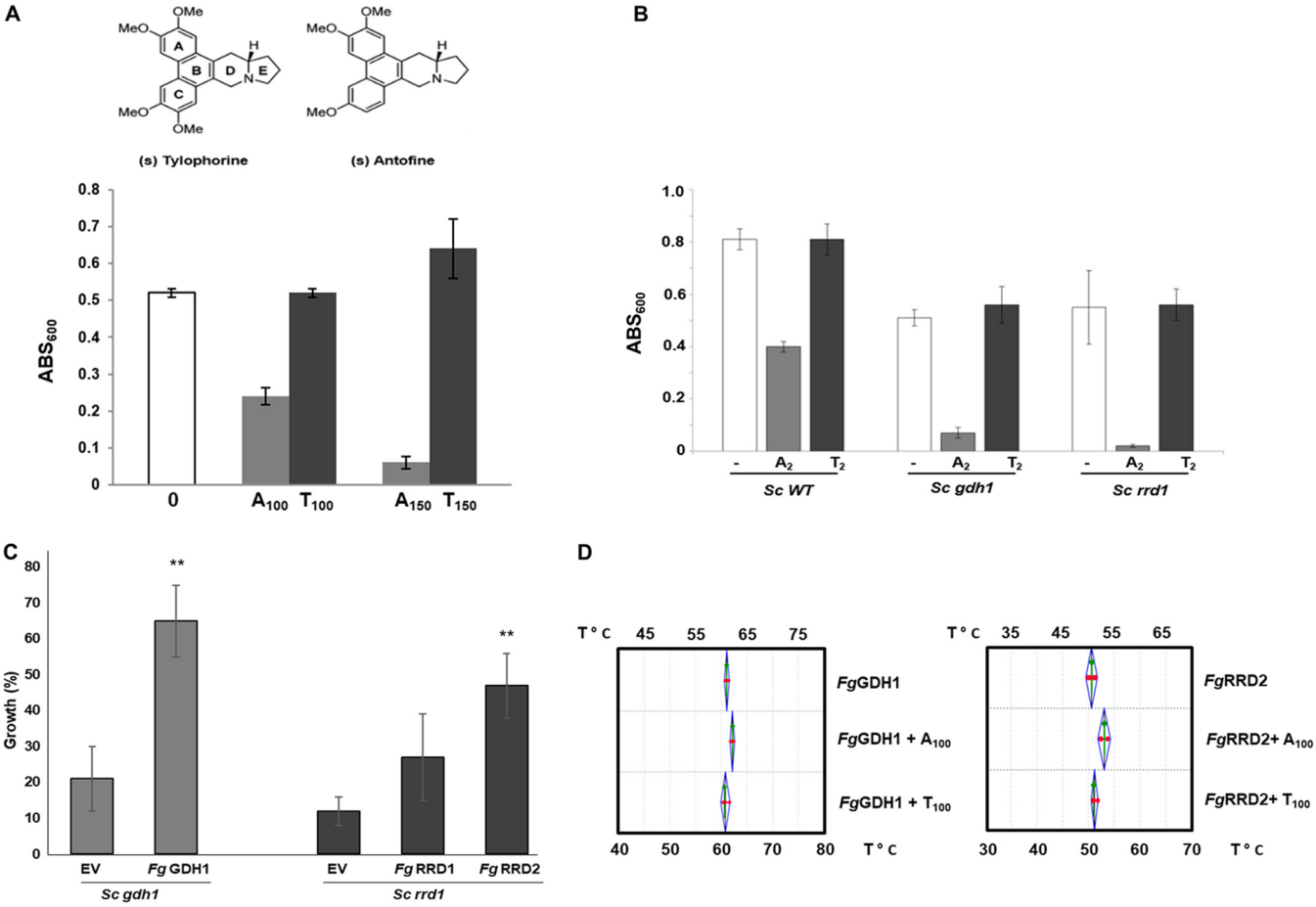

FIG 1 Antofine inhibits growth of *F. graminearum* and targets GDH1 and RRD1. (A). Wild-type *F. graminearum* (*Fg*) spores were coincubated with 100 μg/ml of antofine (A_{100}), tylophorine (T_{100}), or solvent control (−), and mycelial growth was monitored by absorbance at 600 nm (ABS_{600}). Results are representative of five biological replicates. The chemical structures of tylophorine and antofine are shown. (B) Growth of wild-type *S. cerevisiae* (*Sc WT*) or *Scgdh1* and *Scrrd1* mutants in the presence of 2 μg/ml antofine (A_2), tylophorine (T_2), or solvent control (−) was monitored by absorbance at 600 nm (ABS_{600}). Values represent the average of three technical replicates with standard deviation. The results are representative of four biological replicates. (C) *F. graminearum* GDH1 and RRD2 complement antofine hypersensitivity to the *Scgdh1* and *Scrrd1* mutants, respectively. *Fg GDH1* (FGSG_07174) was expressed in the *Scgdh1* mutant, and *FgRRD1* (FGSG_09229) and *Fg*RRD2 (FGSG_01092) were expressed in the *S. cerevisiae Scrrd1* mutant. Empty vectors (EVs) were used as controls. Expression of *FgGDH1* and *FgRRD1* was induced by galactose and was monitored in the absence and presence of 2 μg/ml antofine. Values represent average percentage of growth with respect to growth in the absence of antofine of three technical replicates with standard deviation. (D) Thermal shift assays using 1 mg/ml of purified *Fg*GDH1 and *Fg*RRD2 proteins in the absence and presence of antofine (A_{100}), and tylophorine (T_{100}) at 100 μg/ml. Results are representative of two independent biological replicates with four technical replicates in each experiment.

a sublethal concentration (2 μg/ml) of antofine (see Fig. S3A in the supplemental material), we conducted an HIP screen on ~6,000 yeast heterozygous strains and identified three heterozygous strains that were hypersensitive to antofine. While wild-type (WT) yeast growth was inhibited by 2.5% at 2.0 μg/ml of antofine (~4 μM), the 3 heterozygous mutants YOR375C, YBR095C, and YIL153W displayed 23, 15.5, and 12.5% growth inhibition, respectively (Fig. S3B). The *Saccharomyces cerevisiae* glutamate dehydrogenase gene (*ScGDH1*; YOR375C) has a homologue in *F. graminearum* (FGSG_07174) with 73% identity, and the *ScRRD1* gene (resistant to rapamycin deletion 1; YIL153W) has two homologues in *F. graminearum*, FGSG_09229 (*FgRRD1*) and FGSG_01092 (*FgRRD2*), with identities of 38 and 32%, respectively (13). The third target identified in yeast YBR095C showed a weak homology (18% identity) with *F. graminearum* gene FGSG_08612, and the homology between these proteins was not contiguous. Therefore, we pursued *FgGDH1*, *FgRRD1*, and *FgRRD2* for further characterization as putative targets of antofine. Note that both *Scgdh1* and *Scrrd1* mutant strains displayed no hypersensitivity to the negative-control tylophorine (Fig. 1B).

To determine if *F. graminearum* genes could complement yeast mutants, we ex-

pressed *Fg*RRD1 (FGSG_09229) and *Fg*RRD2 (FGSG_01092) in the *S. cerevisiae* YIL153 mutant strain and expressed *FgGDH1* (FGSG_07174) in the *S. cerevisiae* YOR375C mutant strain. *Fg*GDH1 was able to partially complement the antofine sensitivity of the *Scgdh1* mutant strain (Fig. 1C). Interestingly, *Fg*RRD2 ($P < 0.01$) but not *Fg*RRD1 was able to partially rescue antofine sensitivity in the *Scrrd1* mutant strain and was therefore chosen for further analysis (Fig. 1C). To test if *Fg*GDH1 and *Fg*RRD2 are direct targets of antofine, both genes were cloned and expressed, and the purified protein (see Fig. S4 in the supplemental material) was used in thermal shift assays (TSAs) (17, 18). TSA determines a shift in the melting temperature (T_m) of a protein upon binding to a ligand, measured by changes in light scattering or fluorescence. The T_m of *Fg*GDH shifted from 61°C to 62.4°C in the presence of 100 μg/ml of antofine (Fig. 1D; $+A_{100}$); however, in the presence of 100 μg/ml of tylophorine, the T_m did not shift relative to *Fg*GDH alone (Fig. 1D; T_{100}). The TSA also showed that the T_m of purified *Fg*RRD2 shifted from 51°C to 54°C (Fig. 1D; A_{100}) and similar to *Fg*GDH, the shift with tylophorine was negligible compared to that with the protein alone (Fig. 1D; T_{100}). The TSA results indicate that antofine binds both *Fg*GDH and *Fg*RRD2 proteins.

Since antofine inhibited FHB symptoms on wheat (Fig. S2B), we tested whether both antofine targets were associated with fusarium pathogenicity. We deleted *GDH1* and *RRD2* in *F. graminearum* and performed pathology tests on the susceptible wheat variety Roblin. The deletion of *FgGDH1* did not affect the pathogenicity, suggesting that it is not the antofine target responsible for *F. graminearum* virulence (see Fig. S5A in the supplemental material). In contrast, targeted deletion of *FgRRD2* significantly affected the virulence of *F. graminearum* (Fig. S5B). After 15 days postinfection (dpi), the entire wheat head was bleached after inoculation with wild-type *F. graminearum* spores (Fig. S5B; *Fg*), while no such effect was visible after inoculation with the mutant strain (Fig. S5B; *Fg rrd2*). It is likely that growth defects and its inability to produce the mycotoxin deoxynivalenol significantly contributes to the virulence defects (13). Overexpression of *FgRRD2* in the *Fgrrd2* mutant strain (*Fgrrd1*::OE*FgRRD2*) not only restored *F. graminearum* virulence (Fig. S5b; *Fg rrd2*:OE*Fg RRD2*) but also counteracted the effect of antofine (Fig. 2C). These results suggest that although antofine appears to have multiple targets, *Fg*RRD2 is the target responsible for virulence inhibition in *F. graminearum* (13).

The haploid yeast *rrd1* mutant and mutants of the two homologues in the *F. graminearum* strain PH1, *Fgrrd1* and *Fgrrd2,* have been shown to be resistant to the inhibitory effects of rapamycin (12, 13). We confirmed this phenotype for the *Fgrrd2* mutant in our *F. graminearum* strain (DAOM 233423 [Fig. 2]). Wild-type *F. graminearum* spores pretreated with rapamycin at 10 and 20 ng/ml decreased in growth by 50 and 80%, respectively, relative to untreated spores (Fig. 2A; *Fg Wt*). However, no such growth inhibition was observed with the *Fgrrd2* mutant strain exposed to rapamycin (Fig. 2A; *Fg rrd2*). We therefore hypothesized that if antofine antagonizes RRD2, it should chemically phenocopy the rapamycin insensitivity of the *Fgrrd2* mutant. In support of this, growth of wild-type *F. graminearum* spores was monitored in the presence of sublethal doses of antofine (50 and 100 μg/ml [A_{50} and A_{100}, respectively]) and inhibitory concentrations of rapamycin (20 and 50 ng/ml [R_{20} and R_{50}, respectively]) (Fig. 2B). We observed that the inhibitory effects of rapamycin at both doses were suppressed by antofine at 50 μg/ml (Fig. 2B). Antofine at 100 μg/ml suppressed the inhibitory effect of rapamycin at the lower concentration (20 ng/ml) but not at the higher concentration (50 ng/ml), likely due to synergism between antofine and rapamycin toxicity at higher concentrations. Altogether, the results strongly support RRD2 as a direct target of antofine.

RRD is a component of the target of the rapamycin signaling pathway, which is evolutionarily conserved and important for cell growth in eukaryotes (19). In yeast, the rapamycin-sensitive Tor complex 1 (TORC1), in addition to promoting anabolic processes, leads to suppression of stress response pathways (20). This dual role makes this pathway an extremely important subject area of study since its disruption either through mutation or through chemical inhibition can influence numerous diseases, including cancer and diabetes (21). TORC1 mediates these pathways through regula-

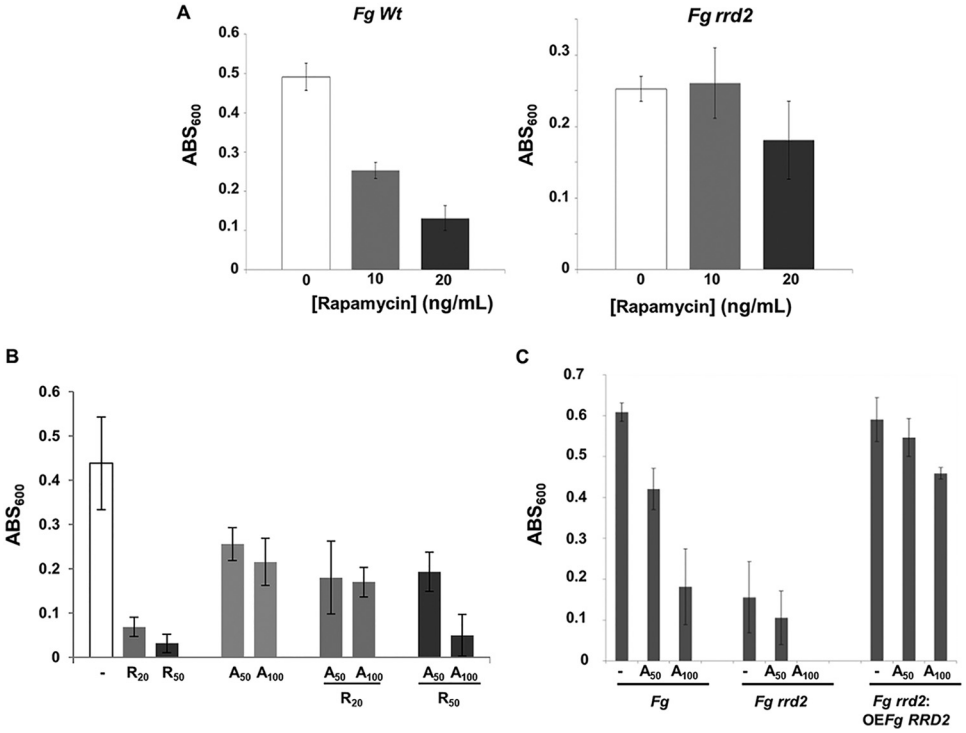

FIG 2 Antofine phenocopies the *rrd2* mutation in *F. graminearum* by suppressing rapamycin toxicity. (A) Growth of the *F. graminearum RRD2* mutant (*Fgrrd2*) is insensitive to rapamycin inhibition. Growth inhibition of wild-type (*Fg Wt*) or RRD2 mutant (*Fg rrd2) F. graminearum* spores coincubated with 10 and 20 ng/ml of rapamycin was monitored by absorbance at 600 nm (ABS_{600}). (B) Growth inhibition of wild-type *F. graminearum* by rapamycin is suppressed by antofine (A_{50} and A_{100}). Growth (optical density at 600 nm [OD_{600}]) of wild-type *F. graminearum* spores was monitored in the presence of rapamycin at concentrations of 20 or 50 ng/ml (R_{20} and R_{50}) alone or in combination with 50 or 100 μg/ml of antofine (A_{50} and A_{100}). (C) Overexpression of RRD2 suppresses antofine toxicity. The mycelial growth of wild-type (*Fg*), *FgRRD2* mutant (*Fg rrd2*), and overexpressor of *RRD2* (*Fg rrd2*:OE*Fg RRD2*) *F. graminearum* strains was monitored by absorbance at 600 nm (ABS_{600}) in the absence (−) and in the presence of 50 and 100 ng/ml of antofine (A_{50} and A_{100}). Values represent the average from three technical replicates with standard deviation. Results are representative of four independent biological replicates.

tion of a set of serine/threonine protein phosphatases, including Sit4, protein phosphatase 2A (PP2A), and Ppg1, which together form the phosphatase-associating protein Tap42 protein complex in a nutrient- and Tor-dependent manner (22). The current model suggests that TORC1 is associated with the Tap42-phosphatase complexes, and upon nutrient stress or rapamycin treatment, the Tap42-phosphatase complex is released from TORC1 (22). This event disassembles the Tap42-phosphatase complex, leading to the activation of the phosphatases and inhibition of Tor activity (19). Therefore, as a positive regulator of phosphatases, Tap42 represents an important regulator of the TOR signaling pathway.

In *F. graminearum*, the interactions between components of the Tap42-phosphatase complex have been demonstrated (11, 13). Specifically, FGSG_09800 (Tap42) interacts with the phosphatases Sit4 (FGSG_01464), Ppg1 (FGSG_05281), and Pp2A (FGSG_09815), protein phosphatase activators RRD1 (FGSG_09229) and RRD2 (FGSG_01092), and a Tap42 interactor protein, Tip41 (FGSG_06963) (Fig. 3A) (11, 13). Mutation of the phosphatases Sit4 and Ppg1, the Tap42 interactor Tip41, or the phosphatase activators RRD1 and RRD2 leads to reduction of virulence of *F. graminearum* (11, 13). Since antofine appears to target RRD2 (FGSG_01092), we tested whether its interactions with Tap42 complex proteins are disrupted by antofine. We performed yeast two-hybrid (Y2H) analysis between *Fg*RRD2 and *Fg*Tap42, *Fg*Sit4, *Fg*Ppg1, *Fg*Pp2A, and *Fg*Tip41 and found that *Fg*RRD2 interacted only with *Fg*Tap42 (see Fig. S6A in the supplemental material). To validate these findings, we quantitatively assessed the interaction between *Fg*Tap42 and *Fg*RRD2 by ONPG (*o*-nitrophenyl-β-D-galactopyranoside) assay (Fig. 3B) (23).

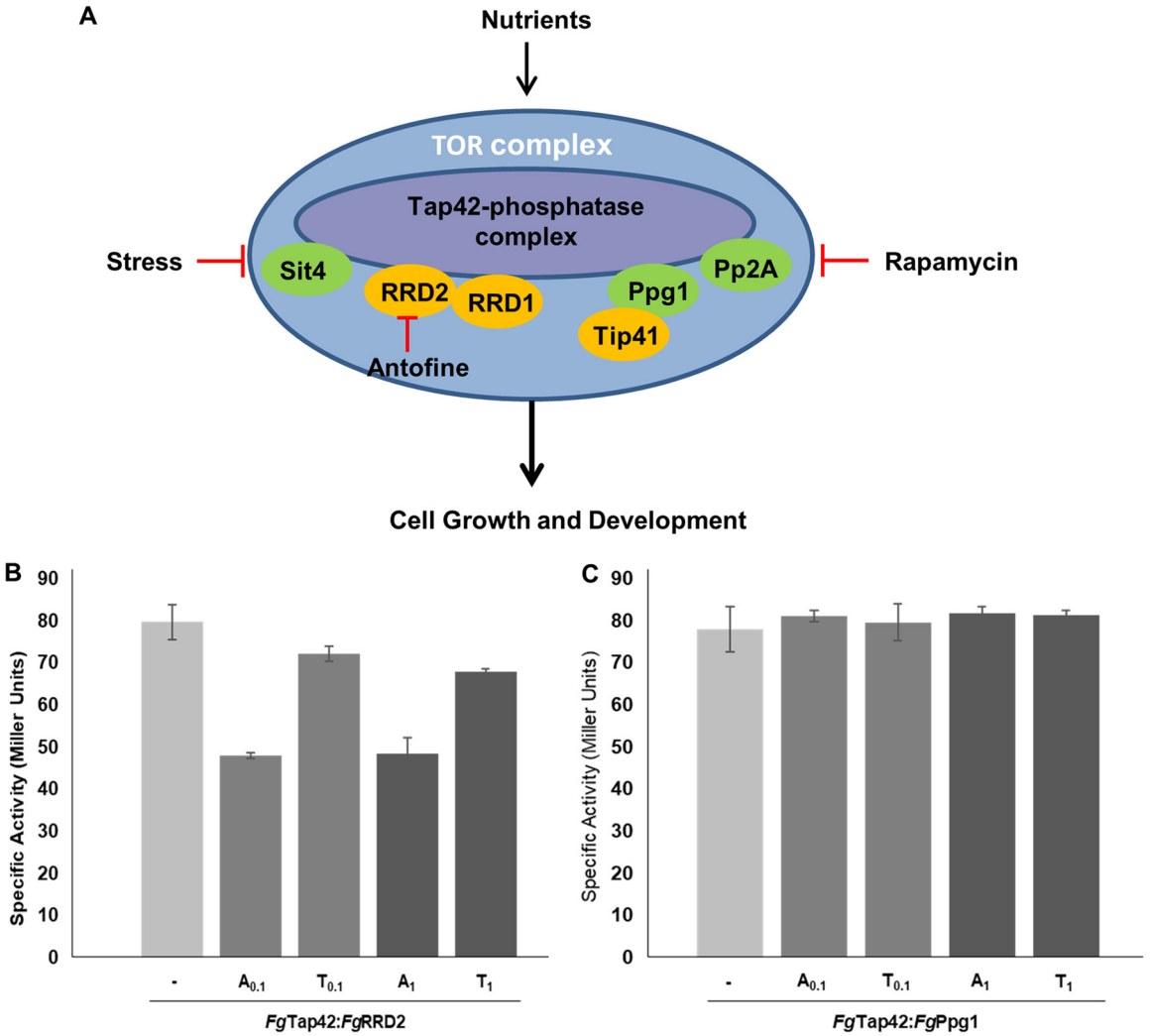

FIG 3 Antofine targets RRD2 and disrupts the Tap42-phosphatase complex in *F. graminearum*. (A) Model representing the TOR complex with components of the Tap42-phosphatase complex highlighting the negative regulation of RRD2 by antofine. The phosphatases are colored green. (B) Antofine specifically disrupts *Fg*Tap42-*Fg*RRD2 protein interaction in the Tap42 complex. The gene pairs *Fg*Tap42 and *Fg*RRD2 and *Fg*Tap42 and*Fg*Ppg1 were expressed in yeast in the absence (−) and in the presence of antofine and tylophorine at 0.1 and 1 μg/ml. The β-galactosidase specific activity (in Miller units) was measured by the ONPG assay (23). (C) The interaction between Tap42 and *Fg*Ppg1 has been demonstrated previously and was used as a positive control (11). Shown is a representative of three independent biological replicates, each with three technical replicates.

The strong interaction between Tap42 and RRD2 was inhibited even at a very low concentration of antofine (0.1 μg/ml [Fig. 3B]), while another interaction between Tap42 and Ppg1 remained intact even at higher concentrations of antofine (1 μg/ml [Fig. 3C]). Inhibition of the *Fg*Tap42-*Fg*RRD2 interaction was relatively specific to antofine ($P < 0.0002$) since inhibition with tylophorine was weak and only significant at the higher concentration tested (1 μg/ml [Fig. 3A]). Finally, we showed that antofine treatment was not deleterious to the accumulation of *Fg*RRD2, *Fg*Tap42, and *Fg*Ppg1 proteins (Fig. S6B). Since RRD binds to Tap42, we hypothesize that disruption of interaction between *Fg*RRD2 and Tap42 by antofine may deregulate the disassembly process of the Tap42-phosphatase complex with TORC1, potentially affecting Tor activation.

In summary, we have identified targets of antofine in *F. graminearum*, one of which (RRD2) is crucial for pathogenicity in wheat. Our finding that the plant-derived compound antofine directly impacts the action of TOR signaling provides an additional tool to dissect this complex signaling pathway and a potential lead compound for integrative pest management programs in crop protection. In addition to rapamycin, other

inhibitors of the TOR pathway such as PP242, which acts as a competitive inhibitor for the ATP binding site of mammalian TOR, have been proposed for therapeutic use (24). More recently, PP242 was also used to inhibit the plant Tor kinase and reduce *F. graminearum* disease development in *Arabidopsis* (25). A similar increase in resistance to pathogens was observed when signaling from the TOR pathway was attenuated in *Arabidopsis* with a mutation in the *Raptor* gene, a direct target of the Tor kinase (26). However, the same study showed that manipulation of the TOR pathway could have unintended negative effects on plant growth, which presents an obvious hurdle to targeting this pathway for crop protection.

Large-scale fungicide use in agriculture is leading to emergence of multidrug resistance (MDR) in fungal strains, characterized by partial to complete resistance to fungicides (10). In this context, combinatorial drug application is one approach that can be used to combat MDR pathogens in agriculture. Such an approach is common in treating human diseases such as HIV and malaria and is also a strategy to combat deadly human fungal pathogens, such as *Candida*, *Aspergillus*, and *Cryptococcus*, and block the emergence of resistance (27, 28). The latter study showed that the small molecule beauvericin increased efficacy of azole-derived compounds through the inhibition of a multidrug efflux pump and the TOR signaling pathway (28). Similarly, a checkerboard analysis between antofine and existing fungicides could reveal concentrations of antofine that are benign to humans but can increase the efficacy of other commonly used azole-derived fungicides used in agriculture (29).

MATERIALS AND METHODS

Purification and confirmation by NMR of antofine. Root tissues of *Vincetoxium rossicum* were harvested, vacuum desiccated, and crushed in EtOAc. The crude extract was filtered, concentrated by rotary evaporator, and dissolved in 0.01 M HCl. The pH was reduced to 2.0 with 1 M HCl and the solution partitioned with EtOAc. The organic fraction was concentrated by rotary evaporator and dried for storage. The pH of the aqueous fraction was increased to 10 with 1 M NH_4OH and partitioned with EtOAc. The alkaline fraction containing antofine was concentrated by rotary evaporator, dissolved in pure acetonitrile (ACN), and injected into a 250- by 10-mm 5-μm 120-Å C_{18} reverse-phase semipreparatory column (ACE-121-2510; Advanced Chromatography Technologies). The column was preequilibrated in a gradient (5% ACN in water to 75% ACN in water) over 20 min at 10 ml/min. Antofine was eluted in 75% ACN–distilled water (dH_2O) in 10-ml fractions for 20 min. An aliquot of 2 ml from each sample was dried using a SpeedVac (SVC-100H; Savant) and suspended in 200 μl methanol (MeOH). A 10-μl aliquot was spotted onto a sterile 6-mm filter disc. The discs were placed amended side down on petri dishes containing 2% YPD (yeast extract-peptone-dextrose) agar evenly spread with $\sim 1.0 \times 10^6$ CFU of *S. cerevisiae* BY4741 and incubated at 30°C overnight. The fractions that demonstrated an inhibition zone were pooled and dried using a rotary evaporator. The pellet was suspended in MeOH and spotted onto a glass-backed silica thin-layer chromatography (TLC) plate (5715-7; EMD Chemicals). Compounds were separated by TLC with two consecutive migrations of 60:40 EtOAc-MeOH and traced by illumination under shortwave (254-nm) UV light. Each band was scraped from the silica plate and recovered using MeOH. The MeOH was removed by rotary evaporator, and the recovered compounds were solubilized in $CHCl_3$ and tested for activity as described before. Purified antofine was subjected to ^{1}H nuclear magnetic resonance (NMR) for confirmation. The NMR spectrum was recorded on a Bruker Avance 400-MHz NMR spectrometer. The sample was recorded using $CDCl_3$ as the solvent, purchased from Cambridge Isotope Laboratories, Inc. The reference peak was set using the known residual solvent peak of $CDCl_3$ at 7.26 ppm. The NMR spectrum was compared to the known spectrum of antofine (30).

Identification of antofine targets in yeast by haploinsufficiency profiling. The Yeast Heterozygous Knock-Out collection (Open Biosystems; GE Healthcare, USA), along with the diploid wild-type strain (BY4743), was copied to solid 2% YPD agar amended with 150 μg/ml G418, contained in an Omniwell plate (Nunc catalog no. 242811), using a 96-pin replicator (Nunc catalog no. 250520) and the OmniTray copier (Nunc catalog no. 250555) and incubated overnight at 30°C. The initial screen was initiated with antofine (0.75 μg/ml) and incubated for 24 h at 30°C. The plates were scanned as a grayscale image (Epson Perfection V750 Pro) and processed with the Epson Scan version 3.24A scanning software at a 300-dpi resolution. The initial screen was repeated 6 times at antofine concentrations of 2.75, 2.5, 2.0, and 1.25 μg/ml, with a final concentration of methanol at 0.01%. The results of the initial screens were analyzed together using the Screen Mill analysis package, and all mutants that received a *P* value of <0.05 were selected for further analysis (31).

Our initial screen yielded 873 potential candidates. To further narrow the list of candidates, we employed a liquid-based analysis. Briefly, each mutant was grown to an absorbance at 600 nm (ABS_{600}) of ~ 5.0, and 10 μl of this new cell suspension was transferred to a new 96-well plate containing 190 μl of YPD and bringing the cell density equivalent to an ABS_{600} reading of 0.25 ($\sim 5.0 \times 10^6$ CFU/ml), supplemented with 0.20 μg/ml of Antofine. The plate was then loaded into a BioTek Powerwave plate reader, for incubation at 30°C, and then the growth was assessed by ABS_{600} every 10 min over the course of 48 h. The growth for each mutant (with antofine) was then compared to the average growth

calculated for the WT (with antofine), by subtracting the calculated percentage of WT growth from the calculated percentage of growth for the mutant, where a positive result signified the mutant grew better than the WT under experimental conditions, and a negative result signified the mutant grew poorer than the WT when antofine was present. We used 10% as the cutoff for growth differences. This analysis yielded 16 mutants sensitive to antofine.

To confirm the observed effect of antofine, 16 antofine-sensitive mutants were further screened with three concentrations of antofine (2.5, 2, and 1.5 μg/ml) in triplicate. This was repeated three times. After analysis, three yeast mutants (YBR095C, YOR375C, and YIL153W) showed a consistent sensitive phenotype to antofine.

ScreenMill analysis. The differences in colony growth were assessed by the ScreenMill growth measurement and analysis software suite (31). Briefly, each plate is scanned and then analyzed using the colony measurement engine, which detects each colony and assigns each a numerical value based upon its circularity and size. The file output is then input into the data review engine. A web-based application normalizes raw screen data and provides the user with an opportunity to manually select data for exclusion from analysis. The normalized data are used to calculate *P* values by *t* test for parametric data or the Mann-Whitney test for nonparametric data.

Construction of *F. graminearum Fggdh1* and *Fgrrd2* mutant strains and the *Fgrrd2*::OE*FgRRD2* overexpression strain. *F. graminearum* wild-type strain DAOM 233423 (NRRL29169) was provided by C. Babcock of the Canadian Collection of Fungal Cultures (CCFC/DAOM), Agriculture and Agri-Food Canada, Ottawa. Macroconidia were used as the inoculum for all experiments and were produced in a liquid carboxymethyl cellulose medium (32). All of the plasmids were constructed by the USER (uracil-specific excision reagent) technique and outlined (see Fig. S7 in the supplemental material) (33). The deletion of *FgGDH* (FGSG_07174) and *FgRRD2* (FGSG_01092) was performed by PCR amplification of the two homologous recombination sequences (HRSs) for each gene. HRS1 for FGSG_07174 was obtained with primer sets Fg 07174 USER Up-F/R, and HRS1 for FGSG_01092 was obtained with Fg 01092 USER Up-F/R. HRS2 for FGSG_07174 was obtained with primer sets Fg 07174 USER Dn-F/R, and HRS2 for FGSG_01092 was obtained with Fg 01092 USER Dn-F/R. PCR products HRS1 and HRS2 were introduced into the pRF-HU2 vector with hygromycin (Hyg) as the selection marker. The *Fgrrd2*::OE*FgRRD2* overexpression strain was constructed by introducing FGSG_01092 cDNA into the pRF-GUE vector with Geneticin as the selection marker (Gen). The cDNA was amplified by the primer set Fg 01092 GUE_F/R. The *F. graminearum* mutants were screened for the presence and absence of FGSG_07174 and FGSG_01092 with primer sets Fg 07174 Orf F/R and Fg 01092 Orf F/R, respectively. The presence of the *gpdA* promoter in the *Fgrrd1*::OE*Fg RRD1*strain was confirmed by the primer set Gpd Pro F and Fg 01092 Orf R. The sequences of the primers are listed in Table S1 in the supplemental material. Touchdown PCR conditions were used to confirm *F. graminearum* transgenic strains: 100 ng of genomic DNA for 8 cycles at 63 to 55°C and for 22 cycles at 55°C. We verified the copy number in the mutant strains by quantitative real-time PCR (qRT-PCR) analyses (Fig. S7G). Briefly, the analyses were performed with the primer set Fg 01092 qPCR F/R for FGSG_01092 and the primer set Fg 07174 F/R for FGSG_07174 and normalized with a known single-copy gene coding for glyceraldehyde-3-phosphate dehydrogenase, *GAPDH* (FGSG_16627), using the primer set Fg 16627 F/R (Table S1) (34). All samples were assessed in triplicate using the QuantStudio3 (Applied Biosystems, USA).

RNA extraction and cDNA library from *F. graminearum*. *F. graminearum* strains were grown in a mixture of 56 mM NH_4Cl, 8.1 mM $MgSO_4{\cdot}7H_2O$, 0.23 mM $FeSO_4{\cdot}7H_2O$, 14.7 mM KH_2PO_4, 2 g/liter peptone, 2 g/liter yeast extract, 2 g/liter malt extract, and 111 mM glucose for 24 h, and total RNA was extracted from mycelia using TRIzol reagent (Invitrogen), purified using the InviTrap Spin cell RNA minikit (Stratec, Germany), and then converted into cDNA (1 μg) using the Applied Biosystems high-capacity cDNA reverse transcription kit. RT-PCRs were similar to the touchdown PCR conditions mentioned before.

Growth curve assays with inhibitors. One thousand spores from *F. graminearum* wild-type (*Wt*), ΔFGSG 07174 and ΔFGSG 01092 mutant strains, and the *Fgrrd2*::OE*FgRRD2*strain were inoculated in 200 μl GYEP medium (0.1% KH_2PO_4, 0.05% $MgSO_4{\cdot}7H_20$, 0.05% KCl, 0.02% [vol/vol] trace element solution, and 0.01% sucrose). The spore germination assay was set up in 96-well microtiter plates (Corning 3632), and growth was monitored over a 48-h period at 600 nm using the FLUOstar Optima plate reader (BMG Labtech, USA) in a final volume of 200 μl. We assessed the germination and growth of various numbers of spores (250, 500, and 1,000) by absorbance (λ = 600 nm) and visualization at numerous time points with a Zeiss AxioImager M2 microscope (Carl Zeiss Canada, Toronto, Ontario) (Fig. S1B). An absorbance reading of ~0.5 was the same for all the spore concentrations at 48 h. Therefore, we used 48 h as the endpoint measurement for all of the fusarium spore germination/growth assays. All yeast strains were grown overnight in YPD (yeast extract-peptone-dextrose) at 30°C with shaking at 200 rpm overnight. Cells were diluted to an ABS_{600} of 0.5 and used in growth curve assays. The growth was monitored over a 24-h period at 600 nm using the FLUOstar Optima plate reader as described before. The inhibitors were dissolved in 100% methanol and were used at the indicated concentrations in a 1% final concentration of methanol in all of the liquid assays.

Purification of *Fg*GDH (FGSG_07174) and *Fg*RRD1 (FGSG_01092) from yeast. Both FGSG_07174 and FGSG_01092 were cloned into the pYES-DEST 52 Gateway destination plasmid vector by LR clonase reaction (Life Technology, USA). Plasmids were transformed into yeast knockout strains YOR375C and YIL153W, respectively. The complemented yeast was grown in 5 ml of Sabouraud dextrose (SD) medium lacking uracil in the presence of 2% glucose and antibiotic selection with G418 (Sigma) overnight at 30°C. Yeast cells were transferred in a 1:100 ratio to 30 ml of inducing medium with 2% galactose, 1% raffinose, and G418 overnight at 30°C. Yeast cells then were harvested by centrifugation at 2,700 × *g* for 10 min. The resulting yeast pellet was processed for protein extraction. The His-tagged proteins were purified

using the Clontech His-tagged purification miniprep kit. Yeast pellet containing the His-tagged protein was thawed in 1 ml X-tractor buffer, 100 μl Zymolyase (5 U/μl; G Biosciences), 40 μl of 25× Roche Complete mini-protease inhibitor cocktail, 10 μl RNase A (20 mg/ml; Sigma), and 5 μl DNase I (10 U/μl; Agilent). The lysate was incubated at 37°C for 1 h and purified according to the manufacturer's instructions with modifications. Briefly, the total lysates were centrifuged at 15,000 rpm to get rid of the cellular debris, and the supernatant was loaded onto the affinity column. After washes with buffer (20 mM Tris [pH 8.0], 30 mM NaCl, 2 mM dithiothreitol [DTT], and protease inhibitor cocktail) containing 20 and 50 mM imidazole, proteins were eluted with buffer containing 500 mM imidazole. Eluates were dialyzed with buffer overnight at 4°C. Glycerol was added to a final concentration of 20%, and the mixture was stored at −20°C until use.

TSAs. Thermal shift assays (TSAs) were performed with purified *Fg*GDH and *Fg*RRD2 proteins. The TSA was performed in Quant Studio 3 (Applied Biosystems) with the Applied Biosystems protein thermal shift dye kit (4461146) in a 20-μl reaction volume containing 1 mg/ml of each protein with or without antofine or tylophorine (Santa Cruz Biotechnologies, USA) at 100 μg/ml (0.1% methanol). The PCR conditions were used according to the manufacturer's instructions, and data were analyzed with Protein Thermal Shift software version 1.3 (Thermo Fisher Scientific). Melting temperature (T_m) data were generated using the Boltzmann method. ΔT_m was calculated by comparing the T_m values for each protein without the inhibitors to those with the inhibitors. Data were collected at 1°C intervals from 25°C through 99°C and are shown in the replicate result plot view of the Protein Thermal Shift software.

***Fusarium* infection assay.** Each strain was assessed for the ability to infect susceptible *Triticum aestivum* (cv. Roblin). Wheat heads (10 heads per strain) were point inoculated at mid-anthesis with each strain at 100,000 spores/ml in a volume of 10 μl (1,000 spores). Spores were inoculated between the palea and lemma of a single wheat spikelet. Plants were grown at 25°C for 16-h days with misting every hour for 30 s. After 48 h, misting was reduced to a duration of 30 s every 4 h. Infection was scored by counting the number of visibly infected spikelets at days 5, 10, and 15 (32).

Yeast two-hybrid and ONPG assays. The coding sequences of *Fg*Tap42, *Fg*RRD2, *Fg*Tip41, *Fg*Pp2A, and *Fg*Ppg1 from *F. graminearum* were synthesized and cloned into the pDONR vector (General Biosystems, Morrisville, NC). The genes were subcloned into the yeast vectors pJG4-5 (activation domain B42) and pEG202 (DNA binding domain LexA) by Gateway LR Clonase II reaction (Thermo Fisher Scientific). Yeast two-hybrid plasmid pairs were transformed into *S. cerevisiae* strains RFY206 and EGY48, before mating and selection on synthetic medium lacking histidine, uracil, and tryptophan. Two independent yeast colonies containing both pJG4-5 and pEG202 for each gene pair were selected for interaction, and the interaction was quantified by a β-galactosidase activity assay with ONPG (23). Interaction was monitored in the presence of either antofine or tylophorine (0, 0.1, and 1 μg/ml). Three independent experiments were performed, using corresponding empty vectors as negative controls. All the yeast strains were grown as described before in the purification of *Fg*GDH1 and *Fg*RRD1, except the induction with galactose was limited to 1 h. To ensure that expressed proteins were not affected by antofine, extracts from noninduced and induced cultures (±antofine or tylophorine) were subjected to Western blot analyses. Proteins were extracted by 2 M LiAc and 0.4 M NaOH followed by boiling in Laemmli buffer. Twenty micrograms of protein from each sample was separated on a 10% SDS-PAGE gel, and the blots were probed with LexA antibodies for detection of *Fg*Tap42 (Millipore Sigma, USA) and hemagglutinin (HA) antibodies (Roche, Germany) to detect both *Fg*RRD2 and *Fg*Ppg1 proteins. Proteins were detected by the ECL enhanced chemiluminescence substrate (Lumigen ECL Ultra; TMA-6).

SUPPLEMENTAL MATERIAL

Supplemental material for this article may be found at https://doi.org/10.1128/mBio.00792-19.

FIG S1, TIF file, 0.7 MB.
FIG S2, TIF file, 0.7 MB.
FIG S3, TIF file, 0.5 MB.
FIG S4, TIF file, 0.8 MB.
FIG S5, TIF file, 0.6 MB.
FIG S6, TIF file, 1.9 MB.
FIG S7, TIF file, 0.8 MB.
TABLE S1, DOCX file, 0.1 MB.

ACKNOWLEDGMENTS

This work is supported by an NSERC Discovery grant to D.D.
We thank Shea Miller for microscope use.

REFERENCES

1. Stærk D, Nezhad KB, Asili J, Emami SA, Ahi A, Sairafianpour M, Jaroszewski JW. 2005. Phenanthroindolizidine alkaloids from *Vincetoxicum pumilum*. Syst Ecol 33:957–960. https://doi.org/10.1016/j.bse.2005.01.004.
2. Gao W, Lam W, Zhong S, Kaczmarek C, Baker DC, Cheng YC. 2004. Novel mode of action of tylophorine analogs as antitumor compounds. Cancer Res 64:678–688. https://doi.org/10.1158/0008-5472.CAN-03-1904.
3. Min H-Y, Chung H-J, Kim E-H, Kim S, Park E-J, Lee SK. 2010. Inhibition of cell growth and potentiation of tumor necrosis factor-α (TNF-α)-induced

apoptosis by a phenanthroindolizidine alkaloid antofine in human colon cancer cells. Biochem Pharmacol 80:1356–1364. https://doi.org/10.1016/j.bcp.2010.07.026.
4. Song J, Kwon Y, Kim S, Lee SK. 2015. Antitumor activity of phenanthroindolizidine alkaloids is associated with negative regulation of Met endosomal signaling in renal cancer cells. Chem Biol 22:504–515. https://doi.org/10.1016/j.chembiol.2015.03.011.
5. Oh J, Kim GD, Kim S, Lee SK. 2017. Antofine, a natural phenanthroindolizidine alkaloid, suppresses angiogenesis via regulation of AKT/mTOR and AMPK pathway in endothelial cells and endothelial progenitor cells derived from mouse embryonic stem cells. Food Chem Toxicol 107:201–207. https://doi.org/10.1016/j.fct.2017.06.036.
6. Mogg C, Petit P, Cappuccino N, Durst T, McKague C, Foster M, Yack JE, Arnason JT, Smith ML. 2008. Tests of the antibiotic properties of the invasive vine *Vincetoxicum rossicum* against bacteria, fungi and insects. Biochem Syst Ecol 36:383–391. https://doi.org/10.1016/j.bse.2008.01.001.
7. Windels CE. 2000. Economic and social impacts of *Fusarium* head blight: changing farms and rural communities in the Northern Great Plains. Phytopathology 90:17–21. https://doi.org/10.1094/PHYTO.2000.90.1.17.
8. Edwards SG, Godley NP. 2010. Reduction of Fusarium head blight and deoxynivalenol in wheat with early fungicide applications of prothioconazole. Food Addit Contam Part A Chem Anal Control Expo Risk Assess 27:629–635. https://doi.org/10.1080/19440040903515942.
9. Matthies A, Walker F, Buchenauer H. 1999. Interference of selected fungicides, plant growth retardants as well as piperonyl butoxide and 1-aminobenzotriazole in trichothecene production of *Fusarium graminearum* (strain 4528) *in vitro*. J Plant Dis Prot 106:198–212.
10. Popeil D, Dawidziuk A, Koczyk G, Mackowiak A, Marcinkowska K. 2017. Multiple facets of response to fungicides—the influence of azole treatment on expression of key mycotoxin biosynthetic genes and candidate resistance factors in the control of resistant *Fusarium* strains. Eur J Plant Pathol 147:773–785. https://doi.org/10.1007/s10658-016-1042-3.
11. Yu F, Gu Q, Yun Y, Yin Y, Xu J-R, Shim W-B, Ma Z. 2014. The TOR signaling pathway regulates vegetative development and virulence in Fusarium graminearum. New Phytol 203:219–232. https://doi.org/10.1111/nph.12776.
12. Douville JM, David J, Lemieux KM, Gaudreau L, Ramotar D. 2006. The *Saccharomyces cerevisiae* phosphatase activator RRD1 is required to modulate gene expression in response to rapamycin exposure. Genetics 172:1369–1372. https://doi.org/10.1534/genetics.105.046110.
13. Liu Z, Liu N, Jiang H, Yan L, Ma Z, Yin Y. 2018. The activators of type 2A phosphatases (PP2A) regulate multiple cellular processes via PP2A-dependent and -independent mechanisms in *Fusarium graminearum*. Mol Plant Microbe Interact 31:1121–1133. https://doi.org/10.1094/MPMI-03-18-0056-R.
14. Wu C-M, Yang C-Y, Lee Y-Z, Chuang T-H, Wu P-L, Chao Y-S, Lee S-J. 2009. Tylophorine arrests carcinoma cells at G1 phase by downregulating cyclin A2 expression. Biochem Biophys Res Commun 386:140–145. https://doi.org/10.1016/j.bbrc.2009.05.138.
15. Kwon Y, Song J, Lee H, Kim E-Y, Lee K, Lee SK, Kim S. 2015. Design, synthesis, and biological activity of sulfonamide analogues of antofine and cryptopleurine as potent and orally active antitumor agents. J Med Chem 58:7749–7762. https://doi.org/10.1021/acs.jmedchem.5b00764.
16. Giaever G, Flaherty P, Kumm J, Proctor M, Nislow C, Jaramillo DF, Chu AM, Jordan MI, Arkin AP, Davis RW. 2004. Chemogenomic profiling: identifying the functional interactions of small molecules in yeast. Proc Natl Acad Sci U S A 101:793–798. https://doi.org/10.1073/pnas.0307490100.
17. Huynh K, Partch C. 2015. Analysis of protein stability and ligand interactions by thermal shift assay. Curr Protoc Protein Sci 79:28.9.1–28.9.14. https://doi.org/10.1002/0471140864.ps2809s79.
18. Andreotti G, Monticelli M, Cubellis MV. 2015. Looking for protein stabilizing drugs with thermal shift assay. Drug Test Anal 7:831–834. https://doi.org/10.1002/dta.1798.
19. González A, Hall MN. 2017. Nutrient sensing and TOR signaling in yeast and mammals. EMBO J https://doi.org/10.15252/embj.201696010.
20. De Virgilio C. 2012. The essence of yeast quiescence. FEMS Microbiol Rev 36:306–339. https://doi.org/10.1111/j.1574-6976.2011.00287.x.
21. Ma EH, Jones RG. 2016. Cell growth. (TORC)ing up purine biosynthesis. Science 351:670–671. https://doi.org/10.1126/science.aaf1929.
22. Di Como CJ, Jiang Y. 2006. The association of Tap42-phosphatase complexes with TORC1—another level of regulation in Tor signaling. Cell Cycle 5:2729–2732. https://doi.org/10.4161/cc.5.23.3516.
23. Zhang T, Xu Q, Chen FR, Han QD, Zhang YY. 2004. Yeast two-hybrid screening for proteins that interact with alpha1-adrenergic receptors. Acta Pharmacol Sin 25:1471–1478.
24. Hoang B, Benavides A, Shi Y, Yang Y, Frost P, Gera J, Lichtenstein A. 2012. The PP242 mammalian target of rapamycin (mTOR) inhibitor activates extracellular signal-regulated kinase (ERK) in multiple myeloma cells via a target of rapamycin complex 1 (TORC1)/eukaryotic translation initiation factor 4E (eIF-4E)/RAF pathway and activation is a mechanism of resistance. J Biol Chem 287:21796–21805. https://doi.org/10.1074/jbc.M111.304626.
25. Aznar NR, Consolo VF, Salerno GL, Martínez-Noël GMA. 2018. TOR signaling downregulation increases resistance to the cereal killer *Fusarium graminearum*. Front Plant Signal 13:e1414120. https://doi.org/10.1080/15592324.2017.1414120.
26. De Vleesschauwer D, Filipe O, Hoffman G, Seifi HS, Haeck A, Canlas P, Van Bockhaven J, De Waele E, Demeestere K, Ronald P, Hofte M. 2017. Target of rapamycin signaling orchestrates growth-defense trade-offs in plants. New Phytol https://doi.org/10.1111/nph.14785.
27. Cowen LE. 2013. The fungal Achilles' heel: targeting Hsp90 to cripple fungal pathogens. Curr Opin Microbiol 16:377–384. https://doi.org/10.1016/j.mib.2013.03.005.
28. Shekhar-Guturja A, Gunaherath G, Wijeratne EMK, Lambert J-P, Averette AF, Lee SC, Kim T, Bahn Y-S, Tripodi F, Ammar R, Döhl K, Niewola-Staszkowska K, Schmitt L, Loewith RJ, Roth FP, Sanglard D, Andes D, Nislow C, Coccetti P, Gingras A-C, Heitman J, Gunatilaka AAL, Cowen LE. 2016. Dual action antifungal small molecule modulates multidrug efflux and TOR signaling. Nat Chem Biol 12:867–875. https://doi.org/10.1038/nchembio.2165.
29. Moreno-Martinez E, Vallieres C, Holland SL, Avery SV. 2015. Novel, synergistic antifungal combinations that target translation fidelity. Sci Rep 5:16700. https://doi.org/10.1038/srep16700.
30. Kim S, Lee J, Lee T, Park H-G, Kim D. 2003. First asymmetric total synthesis of (−)-antofine by using an enantioselective catalytic phase transfer alkylation. Org Lett 5:2703–2706. https://doi.org/10.1021/ol0349007.
31. Dittmar JC, Reid RJD, Rothstein R. 2010. ScreenMill: a freely available software suite for growth measurement, analysis and visualization of high-throughput screen data. BMC Bioinformatics 11:353. https://doi.org/10.1186/1471-2105-11-353.
32. Subramaniam R, Narayanan S, Walkowiak S, Wang L, Joshi M, Rocheleau H, Ouellet T, Harris LJ. 2015. Leucine metabolism regulates *TRI6* expression and affects deoxynivalenol production and virulence in *Fusarium graminearum*. Mol Microbiol 98:760–769. https://doi.org/10.1111/mmi.13155.
33. Frandsen RJ, Andersson JA, Kristensen MB, Giese H. 2008. Efficient four fragment cloning for the construction of vectors for targeted gene replacement in filamentous fungi. BMC Mol Biol 9:70. https://doi.org/10.1186/1471-2199-9-70.
34. Nasmith CG, Walkowiak S, Wang L, Leung WWY, Gong Y, Johnston A, Harris LJ, Guttman DS, Subramaniam R. 2011. Tri6 is a global transcription regulator in the phytopathogen *Fusarium graminearum*. PLoS Pathog 7:e1002266. https://doi.org/10.1371/journal.ppat.1002266.